# Rapid, accurate particle tracking by calculation of radial symmetry centers

Raghuveer Parthasarathy

**I introduce an algorithm for subpixel localization of imaged objects based on an analytic, non-iterative calculation of the best-fit radial symmetry center. This approach yields tracking accuracies that are near theoretical limits, similarly to Gaussian fitting, but with orders-of-magnitude faster execution time, lower sensitivity to nearby particles, and applicability to any radially symmetric intensity distribution. I demonstrate the method with several types of data, including super-resolution microscopy images.**

Visualizing the dynamics and spatial distributions of particles yields insights into a vast array of physical and biological systems. For example, imaging fluorophore-conjugated proteins has revealed the processive motions of biomolecular motors[1] and the cellular transport of single viruses[2]; examining the Brownian motion of colloidal particles enables us to discern the rheological properties of complex fluids[3]; and pinpointing single fluorophores allows the reconstruction of super-resolution images of cellular organization[4,5]. For these and other applications, methods have been developed for locating the center of a particle from its digitized image with subpixel precision[6–10], the most accurate of which involve fitting the measured intensity profile to a two-dimensional Gaussian function using nonlinear least-squares algorithms[9] or, more accurately, with a maximum-likelihood estimator[10]. Such fitting suffers from several flaws, however. First, it is slow, requiring numerical iteration to determine optimal parameters. This computation can be prohibitively time-consuming for large data sets. Second, the true particle intensity distribution is, in general, not a Gaussian, but rather the convolution of the object shape with the point-spread function of the imaging system, which may not be precisely known. The fit being optimized, therefore, need not necessarily converge onto the true distribution. Third, a Gaussian fit has many parameters and provides information beyond the desired location of the particle center, such as the amplitude and width of the function, suggesting that much of its computational cost is superfluous to the task of particle localization. These issues lead one to ask whether there exists an approach to particle tracking that is as accurate as Gaussian fitting but that is fast, is efficient and does not assume any particular functional form for the particle intensity distribution.

Neglecting asymmetric optical aberrations (which would complicate any general tracking method), the intensity of an imaged particle is radially symmetric about its center. An algorithm that determines the point of maximal radial symmetry, therefore, would provide the desired localization of the particle center. Although the detection of whole pixels with symmetric surroundings has been the subject of prior study[11], methods for subpixel localization, to the best of my knowledge, have not been developed. In addition to the advantages noted above, such a method would have the additional virtue of general applicability to non–point-like radially symmetric objects: for example, concentric rings derived from holographic microscopy[12].

I provide here such an algorithm that exploits radial symmetry to provide precise particle tracking. I demonstrate that it locates particle centers with subpixel accuracy similar to that of Gaussian fitting but with an execution time that is roughly 100 times faster. The speed is due to a key attribute of the method: an analytic expression for the optimal particle center location, with no iterative, numerical fitting steps. This approach makes use of the fact that for a radially symmetric intensity distribution, a line through any point drawn parallel to the gradient at that point will intersect the particle's center. The distance between the center and any such line is therefore 0. In a noisy, pixelated image, these intersections will not be exact, but we can nonetheless estimate the center as the point that minimizes the total distance between itself and all such lines (**Fig. 1**). It is straightforward to write an algebraic expression for this minimization. I describe this method explicitly (**Supplementary Note**) and characterize its performance using model images, comparing to it Gaussian fitting using both nonlinear least-squares minimization (NLLS) and maximum-likelihood estimators (MLE), centroid calculation[6,9], weighted linearized Gaussian fitting[13] and the FluoroBancroft algorithm[14]. In addition, I compare the realized localization accuracies to the model-independent Cramér-Rao bounds on the maximum attainable accuracy for images with a given information content[10]. I also assess algorithm performance using real data from various experiments.

I first illustrate the performance of radial symmetry–based tracking for simulated images of a point particle with a signal-to-noise ratio (SNr) of 20, equivalent to 3,500 photons at the detector plane, as in **Figure 1** (Online Methods). I plot in **Figure 2a** the $x$ components of errors of center determination for 1,000 images with true centers randomly distributed between ±0.5 pixels in $x$ and $y$; errors in $y$ are similar (**Supplementary Results** and **Supplementary Fig. 1**). The radial symmetry method with local smoothing of the gradient slope (see **Supplementary Note**) gives a mean total error of 0.027 pixels, similar to that of Gaussian fitting using either NLLS, 0.030 pixels, or MLE, 0.025 pixels.

Department of Physics, Materials Science Institute, and Institute for Molecular Biology, University of Oregon, Eugene, Oregon, USA. Correspondence should be addressed to R.P. (raghu@uoregon.edu).

RECEIVED 2 DECEMBER 2011; ACCEPTED 11 MARCH 2012; PUBLISHED ONLINE XX XX 2012; DOI:10.1038/NMETH.XXX

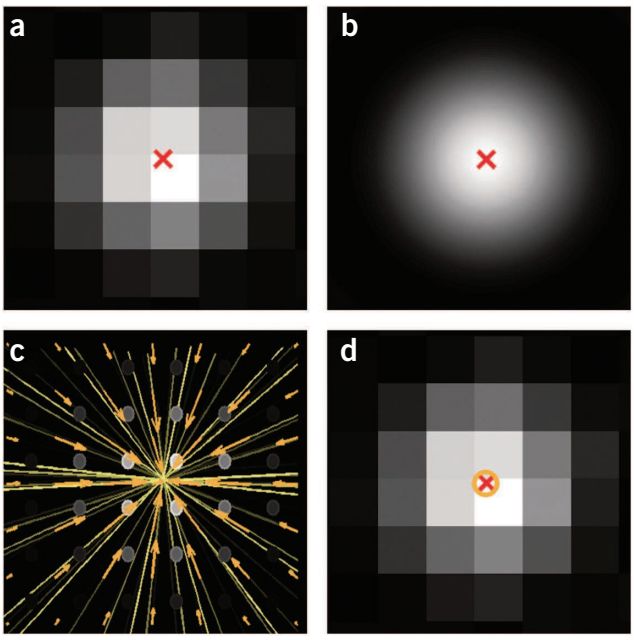


**Figure 1** | Illustration of particle tracking based on radial symmetry. (**a**,**b**) A simulated CCD image of a point source with shot noise (**a**) generated from a noise-free high-resolution simulated image (**b**). The red 'X' indicates the true center. (**c**) The gradient of the intensity (orange arrows) is calculated from the image in **a** at the midpoints between pixel centers. Circles indicate the pixel centers. Yellow lines are drawn through each midpoint, parallel to the gradient. (**d**) The point of minimal distance to the yellow lines in **c**, indicated by the orange circle, provides an accurate, analytically calculable estimate of the particle center location. Q16

The execution time per image of the radial symmetry method is 0.16 ms, whereas those of the Gaussian NLLS and MLE fits are 20.4 and 28.9 ms, respectively—over 100 times longer (Online Methods). I note the contributions of smoothing of the gradient slopes to accuracy and to execution times in the **Supplementary Results** and **Supplementary Figure 1**. The total errors plotted in **Figure 2a** derive from the methods' bias, defined as the slope of the error graphs shown, and from their precision, defined as the scatter about this slope; I provide equations for these and other properties in the Online Methods and compare them for the various localization methods in the **Supplementary Results**. Q6

In **Figure 2b**, I plot the mean error for various tracking methods applied to simulated images spanning a range of SNr (corresponding precision, bias and computation time are plotted in **Supplementary Figs. 2** and **3**). I also include the theoretical lower limit of error, calculated as the Cramér-Rao bound (CRB) of accuracy for a pixelated image with Poisson-distributed noise[10] (see Online Methods). Radial symmetry–based tracking and Gaussian NLLS and MLE fitting are all close to the CRB bound, with the accuracy of the radial symmetry method falling in between the Gaussian NLLS and Gaussian MLE accuracy levels over most of the SNr range examined and surpassing MLE accuracy at very low SNr. Q7

The calculation time per image for the various methods is far slower for Gaussian fitting than for the other, analytically exact, methods (**Supplementary Figs. 2** and **3**). Other than the radial symmetry method, however, the analytically exact methods shown in **Figure 2b** have low accuracy, as does the recently developed FluoroBancroft algorithm discussed in the **Supplementary Results**. The execution times will of course depend on the hardware and the numerical optimization scheme used for Gaussian fitting via either NLLS or MLE. These fitting methods necessarily involve iterative searching for optimal parameters of a nonlinear function, however, and hence are intrinsically more time-consuming than algebraic solutions.

The presence of nearby particles can influence the accuracy of particle localization. Typically, in multiparticle tracking experiments, one localizes individual particles by examining the measured intensity in a small neighborhood. To assess the robustness of particle localization, I consider the case of a second particle whose center may be outside this neighborhood but whose diffracted image extends inside. I plot in **Supplementary Figure 4** the total tracking error as a function of the center-to-center separation of two simulated particles at SNr = 20. As expected, all methods become less accurate as the distance between the particles decreases. For separations smaller than 5 pixels (about 1 wavelength; see Online Methods), however, the radial symmetry–based method has smaller error than Gaussian fitting or centroid

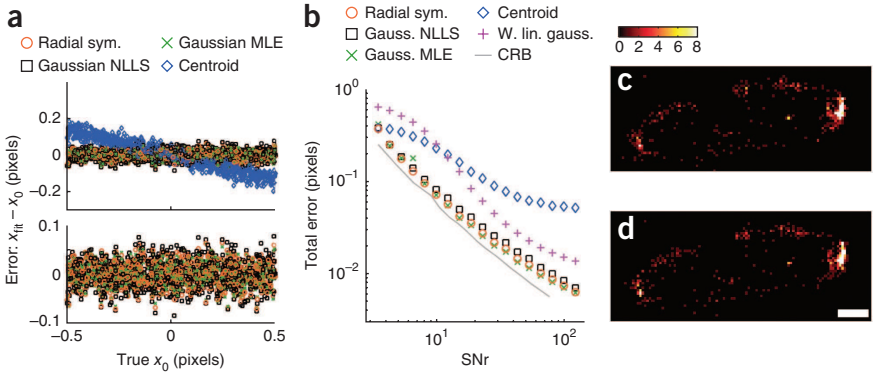


**Figure 2** | Characterizations and applications of radial symmetry–based particle localization. (**a**) Tracking accuracy for various particle localization algorithms applied to simulated particle images with SNr = 20. The *x* component of the difference between the fit-determined and true particle centers is plotted as a function of the true center location. 'Radial sym.' indicates the radial symmetry–based approach introduced here; 'Centroid' indicates centroid finding; 'Gaussian NLLS' and 'Gaussian MLE' refer to Gaussian fitting performed using nonlinear least-squares minimization and maximum-likelihood estimation, respectively. The lower panel shows the same points as the upper panel but with the centroid fit values omitted. (**b**) The localization error from simulated particle images over a range of signal-to-noise ratios (SNr), corresponding to detected photon totals of 100–300,000. Each point denotes the average of 1,000 tests at each SNr. The solid line indicates the Cramér-Rao bound on localization accuracy. (**c**,**d**) Photoactivated localization microscopy images of Tsr-mEos in an *E. coli* bacterium reconstructed from radial symmetry–based (**c**) and Gaussian MLE (**d**) localization of single fluorophore emission images. Each image depicts the number of fluorophores located in 40 nm × 40 nm bins. Scale bar, 500 nm. Color bar, number of fluorophores. Q17 Q18

determination. As above, the radial symmetry–based calculation is about two orders of magnitude faster than Gaussian fitting. It should be noted that all localization methods that are applied to images containing multiple particles must first define regions to analyze, each ideally consisting of only one particle. One can apply various criteria to reject data from regions with non-isolated particles: for example, one can assess the overlap between found object locations before applying a fit. Rejection methods are not intrinsically linked to the fitting method, and existing methods can be applied to radial symmetry–based tracking as well as other approaches.

An important attribute of radial symmetry–based tracking is its applicability to any radially symmetric intensity profile. With no changes to the tracking algorithm, I examined a series of simulated images consisting of two concentric rings (see Online Methods). The resulting accuracy is similar to that from the localization of point particles (**Supplementary Fig. 5**). I also considered asymmetric images with a wide range of SNr values and show that radial symmetry–based tracking and Gaussian fitting methods have similar accuracies (**Supplementary Results**).

The tests above make use of simulated images that mimic the noise and pixelation of experimental data. Simulated images, however, may lack particular distortions or imperfections present in real experiments, thus motivating assessments of performance using actual images. I considered several systems in which the particles of interest are single fluorescent proteins, nanoparticles or micron-scale colloids. (Providers of data and experimental details are described in the Online Methods.) For each of these, the 'true' particle positions are necessarily unknown. One can consider proxy measures of accuracy, however, by comparing radial symmetry–based tracking and Gaussian fitting and by analyzing properties inferred from the tracking output.

Several recently developed super-resolution microscopy techniques operate by accurately determining the locations of discrete fluorophores and reconstructing an image from the set of calculated locations[4,5]. In **Figure 2c**,**d** I plot reconstructed images from radial symmetry–based and Gaussian MLE tracking of photoactivated localization microscopy images of the *Escherichia coli* chemoreceptor Tsr conjugated to the photoactivatable fluorescent protein mEos. In both plots, polarized Tsr clustering is evident. The median deviation between the two methods' particle positions is 0.17 pixels (20 nm). Additional tests on experimental data are described in the **Supplementary Results** and **Supplementary Figure 6**.

I have shown that the radial symmetry of a particle intensity distribution can be exploited to provide an analytic, and hence rapidly calculable, determination of its center location. Consideration of general features of symmetry rather than particular functional forms allows applicability to a wide class of image types: for example, rings and point-like particles. I suggest, therefore, that radial symmetry–based tracking should be useful for a wide variety of imaging-based experiments, especially as the rate of data output by new microscopy methods and new camera technologies continues its impressive increase. More generally, this method suggests a new class of approaches to particle tracking that is based on symmetry considerations. One could consider other types of symmetries beyond radial symmetry: for example, bilateral symmetry can be assessed to track rod-like bacteria or ellipsoidal microparticles.

## METHODS

Methods and any associated references are available in the online version of the paper.

### Accession codes.

*Note: Supplementary information is available in the online version of the paper.*


### ACKNOWLEDGMENTS

I thank H. Deberg, W. Draper, G. Hunter, J. Liphardt, P. Lu, P. Selvin, M. Tjioe, E. Weeks and D. Weitz for sharing and discussing experimental data, and E. Corwin and D. Grier for comments and discussions. This work is supported by the US National Science Foundation (award numbers 0746038 and 1006171).


### AUTHOR CONTRIBUTIONS

R.P. is the sole contributor to this work.

### COMPETING FINANCIAL INTERESTS

The author declares no competing financial interests.

**Published online at http://www.nature.com/doifinder/10.1038/nmeth.2071. Reprints and permissions information is available online at http://www.nature.com/reprints/index.html.**


1. Park, H., Toprak, E. & Selvin, P.R. *Q. Rev. Biophys.* **40**, 87–111 (2007).
2. Brandenburg, B. & Zhuang, X. *Nat. Rev. Microbiol.* **5**, 197–208 (2007).
3. Crocker, J.C. & Hoffman, B.D. *Methods Cell Biol.* **83**, 141–178 (2007).
4. Huang, B., Babcock, H. & Zhuang, X. *Cell* **143**, 1047–1058 (2010).
5. Manley, S., Gillette, J.M. & Lippincott-Schwartz, J. *Methods Enzymol.* **475**, 109–120 (2010).
6. Crocker, J.C. & Grier, D.G. *J. Colloid Interface Sci.* **179**, 298–310 (1996).
7. Rogers, S.S., Waigh, T.A., Zhao, X. & Lu, J.R. *Phys. Biol.* **4**, 220–227 (2007).
8. Thompson, R.E., Larson, D.R. & Webb, W.W. *Biophys. J.* **82**, 2775–2783 (2002).
9. Cheezum, M.K., Walker, W.F. & Guilford, W.H. *Biophys. J.* **81**, 2378–2388 (2001).
10. Abraham, A.V., Ram, S., Chao, J., Ward, E.S. & Ober, R.J. *Opt. Express* **17**, 23352–23373 (2009).
11. Loy, G. & Zelinsky, A. *IEEE Trans. Pattern Anal. Mach. Intell.* **25**, 959–973 (2003).
12. Cheong, F.C. *et al. Opt. Express* **17**, 13071–13079 (2009).
13. Anthony, S.M. & Granick, S. *Langmuir* **25**, 8152–8160 (2009).
14. Andersson, S. *Opt. Express* **16**, 18714–18724 (2008).

## ONLINE METHODS

**Particle localization algorithm.** I provide a detailed derivation of the radial symmetry–based particle localization approach, including analytic expressions that give the particle center, in the **Supplementary Note**.

**Simulated particle images.** I assess the accuracy of particle tracking with simulated images. I model a single fluorescent particle as a point source at some position $(x_0, y_0)$ convolved with a point-spread function (PSF),

$$PSF(r) = \left( \frac{2J_1(v)}{v} \right)^2$$

where $J_1$ is the Bessel function of the first kind of order 1, $v = (2\pi NA\, r) / (\lambda n_w)$, $\lambda = 530$ nm is the wavelength of light, $NA = 1.3$ is the numerical aperture of the objective lens, $n_w = 1.33$ is the index of refraction of water and $r$ is the radial coordinate. The PSF is sampled on a high-resolution grid with a lattice size of 1 nm (0.01 pixels). The convolution of the PSF with a point source is simply a spatially offset PSF, centered at $(x_0, y_0)$.

I show in **Figure 1b** an example of a convolved, noise-free image. I construct the simulated charge-coupled device (CCD) image by integrating the intensity over a coarser lattice corresponding to an 11 × 11 array of CCD pixels of size 100 nm × 100 nm. For Poisson-distributed noise, the peak signal-to-noise ratio is the square root of the number of photons detected at the brightest pixel. To construct an image with a desired SNr, I therefore scaled the intensities such that the peak intensity was equal to the $SNr^2$; this provided the expected intensity (the number of photons) at each pixel. I added a uniform background intensity of ten photons to each pixel. I then replaced the intensity of each pixel by a random number drawn from a Poisson distribution with mean equal to the expected intensity. I show in **Figure 1a**,**d** an example of a simulated image with SNr = 20. The relationship between the SNr and the total number of detected photons in the CCD plane (that is, summed over all pixels) is illustrated in **Supplementary Figure 7**.

**Assessing accuracy.** I computed simulated particles with true centers $(x_0, y_0)$ distributed over the range ±0.5 pixels (50 nm) in each dimension unless otherwise noted. I performed 1,000 simulations and assessments for each set of parameters examined. The average total tracking error is given by

$$e_{\text{total}} = \left\langle e_x^2 + e_y^2 \right\rangle^{1/2}$$

where the angle brackets indicate averages and $e_x$ and $e_y$ are the errors in the calculated $x$ and $y$ positions, respectively:

$$e_x = \left\langle \left( x_{\text{fit}} - x_0 \right)^2 \right\rangle^{1/2}$$

$$e_y = \left\langle \left( y_{\text{fit}} - y_0 \right)^2 \right\rangle^{1/2}$$

where $(x_{\text{fit}}, y_{\text{fit}})$ is the particle center determined by the tracking method being evaluated.

There are two sources of inaccuracy: imprecision in the determination of the particle center at a fixed $(x_0, y_0)$ and systematic error dependent on the position of $(x_0, y_0)$ relative to the pixel center. I define the bias in $x$ as the negative of the slope of a linear regression of $x_{\text{fit}} - x_0$ vs. $x_0$ and the total bias as the average of the biases in $x$ and $y$. Note that the bias is dimensionless, being the 'pixels per pixel' systematic error in center determination. I define the precision in $x$, $\sigma_x$, as the standard deviation of the regression-subtracted error in $x$ (that is, with linearized bias removed), and the total precision is $\sigma = (\sigma_x^2 + \sigma_y^2)^{1/2}$. The bias and precision are illustrated in the **Supplementary Results**.

**Simulated two-particle images.** I similarly constructed simulated images of one particle with a second particle in proximity. I first formed a high-resolution image of two particles modeled as uniform disks with radii of 10 nm on a high-resolution grid with 2-nm spacing, locating the center position of the first particle at a random position in $x, y \in [-0.5, 0.5]$ pixels. I placed the center position of the second particle at some specified distance from the first particle, oriented at a randomly chosen angle in the $xy$ plane. Following convolution of the high-resolution image with the point-spread function, I performed pixelation and incorporated noise as above. I cropped the final simulated images to a centered 7 × 7–pixel (700 × 700–nm) region.

**Simulated two-particle and ring images.** I similarly created simulated images of rings, beginning with high-resolution images of two concentric rings with an annular width of 20 nm, radii randomly selected in the ranges 200–500 nm and 700–1,000 nm, and centers randomly positioned in the range of ±1 pixels (±100 nm) from the image center. I convolved these with the point-spread function noted above and again pixelated the images before incorporating noise.

**Other tracking and assessment methods.** I fit particle images using several methods in addition to the radial symmetry–based determination introduced here. I provide MATLAB code to implement methods 1, 2 and 5 in the **Supplementary Software**.

1. Gaussian fitting via nonlinear least-squares minimization: I fit the intensity to a symmetric, two-dimensional Gaussian function

$$I(x,y) = A \exp\left( -\frac{(x-x_c)^2 + (y-y_c)^2}{2\sigma^2} \right) + B$$

There are five parameters: the amplitude ($A$), offset ($B$), width ($\sigma$) and center $(x_c, y_c)$. I performed the fit by an iterative, nonlinear trust-region method implemented using the Optimization Toolbox of MATLAB (v. 2011a, MathWorks).

2. Gaussian fitting via maximum-likelihood estimation: I determined a maximum-likelihood estimate for a symmetric, two-dimensional Gaussian function

$$I(x,y) = A \exp\left( -\frac{(x-x_c)^2 + (y-y_c)^2}{2\sigma^2} \right) + B$$

as described in ref. 10. This approach considers pixelated, noisy images and maximizes a likelihood estimator which is a function


doi:10.1038/nmeth.2071

of the pixel intensities and a smooth Gaussian form. (Other approaches to maximum-likelihood estimation also exist.) Using the *fminunc* function in the Optimization Toolbox of MATLAB, I numerically minimized the negative of

$$\sum_k \left( z_k \ln\left( I_k\left(A, x_c, y_c, \sigma, B\right)\right) - I_k\left(A, x_c, y_c, \sigma, B\right)\right)$$

where the index $k$ runs over all pixels, $z$ is the pixel intensity and $I$ is the value of the Gaussian function.

3. Centroid: I calculate the $x$ position of the centroid of the image as

$$x_c = \frac{\sum_{ij} x_{ij} I_{ij}}{\sum_{ij} I_{ij}}$$

with the $y$ position calculated analogously. Various researchers have developed methods based on background discrimination and Gaussian filtering to ameliorate the bias inherent in simple centroid finding[6]. Though effective, these approaches add extra parameters and complexity to image analysis and, moreover, do not surpass direct Gaussian fitting in accuracy. As my goal here is to illustrate radial symmetry–based tracking and compare its performance to high-accuracy Gaussian fitting, I do not examine modifications to centroid algorithms.

4. Linearized weighted Gaussian fitting: Gaussian fitting can be linearized, and hence solved analytically, by fitting the logarithm of the particle intensity to a quadratic function of position. The nonlinearity of logarithms enhances the relative weight of low-intensity regions and hence the sensitivity of the fit to noise, a problem for which weighting the intensity by a logarithmically scaled factor was proposed as a solution[13]. I will refer to this method as linearized weighted Gaussian fitting. I caution, however, that linearized Gaussian fitting can easily lead to tracking errors[15]. (Note that ref. 15 has been retracted.)

5. FluoroBancroft algorithm: I implemented the FluoroBancroft algorithm as described in refs. 14 and 16. This approach involves matrix operations on quantities that include the logarithms of the measured intensities and requires an accurate value of the particle width as an input, as discussed in the **Supplementary Results**.

6. CRB limits on tracking precision: As detailed in ref. 10, statistical frameworks exist for determining the Cramér-Rao bounds on the maximum attainable accuracy for localizing images with a given information content, independent of any fitting or localization method. The authors of ref. 10 have made easy-to-use software available for calculating the practical limit of localization accuracy (http://www4.utsouthwestern.edu/wardlab/fandplimittool.asp), which I assessed for the parameters of my simulated images: Airy PSFs pixelated with Poisson-distributed noise, NA = 1.3, wavelength = 530 nm, and so on, as noted above in 'Simulated particle images', with various total photon numbers corresponding to the desired SNr values (Online Methods). The program outputs the lowest attainable error in $x$ and $y$.

**Hardware.** All calculations were run on a Lenovo Thinkpad x220 laptop computer with an Intel i5, 2.5–GHz processor.

**Sources of experimental data.** I assessed the applicability of fitting algorithms to real images using several sets of experimental data graciously shared by various groups.

W. Draper and J. Liphardt (University of California, Berkeley) provided photoactivated localization microscopy data of the bacterial serine receptor Tsr labeled with the photoactivatable fluorescent protein mEos in *E. coli* cells. Fluorophores and imaging parameters were as described in ref. 17. The peak emission wavelength of the activated fluorophores was 581 nm and the CCD image scale was 120 nm per pixel.

H. Deberg and P. Selvin (University of Illinois, Urbana-Champaign) provided fluorescence images of quantum dot–labeled neuromuscular junction–type nicotinic acetylcholine receptors in HEK-293 (human embryonic kidney-293) cells. The peak quantum dot emission wavelength was 655 nm, and the data were captured by a CCD camera at a scale of 107 nm per pixel. Cell culture and imaging were performed as in ref. 18.

M. Tjioe and P. Selvin (University of Illinois, Urbana-Champaign) provided fluorescence images of quantum dot–labeled kinesin traveling along microtubules. The protein construct consisted of 432 residues of kinesin-1 with C-terminal biotin and histidine tags. The peak quantum dot emission wavelength was 655 nm, and the data were captured by a CCD camera at a scale of 107 nm per pixel.

G. Hunter and E. Weeks (Emory University) provided confocal microscopy images of polymethyl methacrylate microspheres labeled with Nile Red (emission peak 582 nm). Other aspects of the particle composition, solvent and imaging were as described in ref. 19. P. Lu and D. Weitz (Harvard University) provided confocal microscopy images of polymethyl methacrylate microspheres labeled with DiIC18 (emission peak 575 nm). Other aspects of the particle composition, solvent and imaging were as described in ref. 20. I calculated two-dimensional pair correlation functions, $g(r)$, from particle position data by calculating the probability distribution of center-to-center separations, $r$, for all particle pairs in a confocal slice (two-dimensional image), normalized by $2\pi r\, dr$, where $dr$ is annular resolution considered, and further normalized by the mean particle concentration. I then averaged these $g(r)$ functions over all slices (roughly 100) in each data set. Q14


15. Harland, C.W., Bradley, M.J. & Parthasarathy, R. *Proc. Natl. Acad. Sci. USA* **107**, 19146–19150; retracted **108**, 14705 (2010).
16. Hedde, P.N., Fuchs, J., Oswald, F., Wiedenmann, J. & Nienhaus, G.U. *Nat. Methods* **6**, 689–690 (2009).
17. Greenfield, D. *et al. PLoS Biol.* **7**, e1000137 (2009).
18. Simonson, P.D. *et al. Biophys. J.* **99**, L81–L83 (2010).
19. Dinsmore, A.D., Weeks, E.R., Prasad, V., Levitt, A.C. & Weitz, D.A. *Appl. Opt.* **40**, 4152–4159 (2001).
20. Lu, P.J. *et al. Nature* **453**, 499–503 (2008).